Effect of Zr and Er on the microstructures, mechanical and electrical properties of Al-0.4Fe alloy

Yaping Kong [a], Zhihong Jia [a, b, f *], Zhipeng Liu [c], Manping Liu [d, *],

Hans J. Roven [e], Qing Liu [a, f]

[a] *International Joint laboratory for Light Alloys (Ministry of Education), College of Materials Science and Engineering, Chongqing University, Chongqing 400044, China*

[b] *Electron microscopy center of Chongqing University, Chongqing 400044, China*

[c] *Zhengzhou Research Institute of CHALCO, Zhengzhou, Henan 450041, China*

[d] *School of Materials Science and Engineering, Jiangsu University, Zhenjiang 212013, China*

[e] *Department of Materials Science and Engineering, Norwegian University of Science and Technology, 7491 Trondheim, Norway*

[f] *Key Laboratory for Light-weight Materials, Nanjing Tech University, Nanjing 210009, China*

*Corresponding authors. Tel. +86 18223013320 (Z.H. Jia), +86 15262987925 (M.P. Liu)

E-mail addresses: zhihongjia@cqu.edu.cn (Z.H. Jia), manpingliu@ujs.edu.cn (M.P. Liu)

Abstract

The effect of Zr and Er on the microstructures, electrical conductivity and mechanical properties of Al-0.4Fe alloy was investigated by using optical microscope (OM), scanning electron microscope (SEM), electron back-scattered diffraction (EBSD), focus ion beam (FIB), transmission electron microscope (TEM) and energy dispersive x-ray spectroscopy (EDS). The grain size of Al-0.4Fe alloy is obviously refined by Zr addition, while Er does not a case. Both Zr and Er could modify the coarse needle-like Al_3Fe particles into fine particles and/or short rods. Zr could promote the formation of primary Al_3Er phase and $Al_3(Zr,Er)$ precipitate in Al-0.4Fe-0.15Zr-0.25Er alloy. Zr and Er co-addition lead to an increase in microhardness, strength with a slight reduction in electrical conductivity. The best combination of strength and electrical conductivity in Al-0.4Fe-0.2Er alloy after cold rolling is obtained as: the yield strength of 145 MPa, the elongation of 8% and the electrical conductivity of 61.2 %IACS. Zr and Er co-addition could also improve the recrystallization-resistant capability of the designed alloy.

Key words： Al-Fe alloy; Zr/Er microalloying; microstructure modification; properties

1. Introduction

Mechanical strength and electrical conductivity are the most important properties of conducting metallic materials used in electrical engineering. Electrical conductivity is very sensitive to the microstructure of the metallic materials, since it is determined by scattering of electrons because of disturbances in the atomic crystal structure,

including thermal vibrations, solutes and crystal defects. Aluminum-iron alloy has been widely used in cables and gained extensive attention due to the interesting combination of electrical conductivity, strength and creep properties. These properties are attributed to low solid solubility of iron in aluminum, the hard and thermostable intermetallics in the Al matrix [1-3]. However, the coarse intermetallics greatly deteriorate the mechanical properties of the alloys because they always serve as crack sources during plastic processing and load-bearing. One method is using modifiers to control the intrinsic crystallization procedure of Al-Fe based alloys, thus effectively improving the nucleation and growth of the primary and eutectic phases during solidification. It was found that the addition of Ce-rich rare-earth refined the primary Al_3Fe phase, formed Al-Ce eutectics in the as-cast alloy, decreased the temperature of the primary Al_3Fe phase, and disturbed the normal crystallization process of eutectic α-Al crystals by decreasing the intrinsic growth along the preferential close-packed $(111)_{Al}$ plane and promoting the growth depending on the sub-closed $(200)_{Al}$ plane [4]. Furthermore, Shi et al. have reported that Al_3Fe, Al_6Fe and Al_3Ce intermetallic phases were found in the RE-modified alloys. The addition of 0.3 wt. % RE modification had the optimized effect on the microstructure and mechanical properties [3].

The addition of Zr/Er to Al alloy has been debated for many years. It was recognized that Zr/Er addition could refine the α-Al dendrites and secondary phases, improving the strength and thermal stability and remaining a high level of electrical conductivity, owing to heterogeneous nucleation (Al_3M, M=Zr, Sc, Er), constitutional supercooling, and interfacial adsorption effects [5-9]. Based on the previous study, Zr

and Er have been the most promising rare earth elements for developing thermally stable and precipitation-strengthened Al alloy [10, 11]. H.C. Fang has reported that the addition of Zr, Er and Cr has synergetic effects on the precipitates, recrystallization and corrosion resistance of Al–Zn–Mg–Cu alloys [12]. Liang et al. have found that Er addition effectively refined the α-Al grain and Al_3Fe phase in Al-2wt. %Fe alloy, due to the primary Al_3Er particle as a favorable heterogeneous nucleation nucleus and Er segregated at the a-Al/Al_3Fe phase interface [13].

Rare earths (RE) elements are special modifiers commonly used in Al alloys. However, the modification effect of Zr and Er on the deformation Al-Fe alloy has not been studied extensively. Therefore, the purpose of this work is to investigate modification of Zr/Er on the microstructures and properties of the Al-0.4Fe alloy.

2. Experimental Procedure

Al-0.4Fe based alloys with single addition and combined addition of Zr and Er were prepared from commercial pure Al (99.9%), Al-20Fe, Al-10Zr and Al-5Er master alloys. The normal compositions of the studied alloys were listed in Table 1. Cast specimens were homogenizing treated at 600 °C for 20h, and then hot-rolled from 48 mm to 7 mm following 480 °C for 2h and subsequently cold-rolled to 2 mm at room temperature.

Electrical conductivity was measured at room temperature, using a HELMUT FISCHER GMBH SIGMASCOPE SMP10 electrical conductivity tester. Microhardness measurements were conducted by a Matsuzawa DVK-1S using a load of 200g for 10s. Each microhardness value is an average of eight separate

measurements. Tensile tests were conducted on a shimadzu mechanical testing machine at a strain rate of 1 mm/min. Tensile samples were taken from the cold rolled sheets.

A Zeiss AURIGA FIB-SEM microscope equipped with the AZtek data acquisition software and the Channel 5 post-processing analysis package was used to investigate microstructure of alloy. The samples were prepared by mechanically grinding, followed by polishing with 9 and 3 μm polishing solution. The electron back-scatter diffraction (EBSD) micrograph was taken in the rolling-normal plane (RD-ND plane). An FEI F20 TEM operated at 200 kV was used to investigate the microstructure. TEM foils were prepared by the FIB method using a ZEISS AURIGA Dual Beam FIB-SEM. The intermetallic particles at grain boundaries were cut out together with the Al matrix.

Table 1 The normal compositions of the studied alloys (wt. %).

Alloys	Fe	Zr	Er	Al
A1	0.4			Balance
A2	0.4	0.1		Balance
A3	0.4		0.2	Balance
A4	0.4	0.1	0.2	Balance

3. Results

3.1 Microstructure

3.1.1 As-cast microstructure

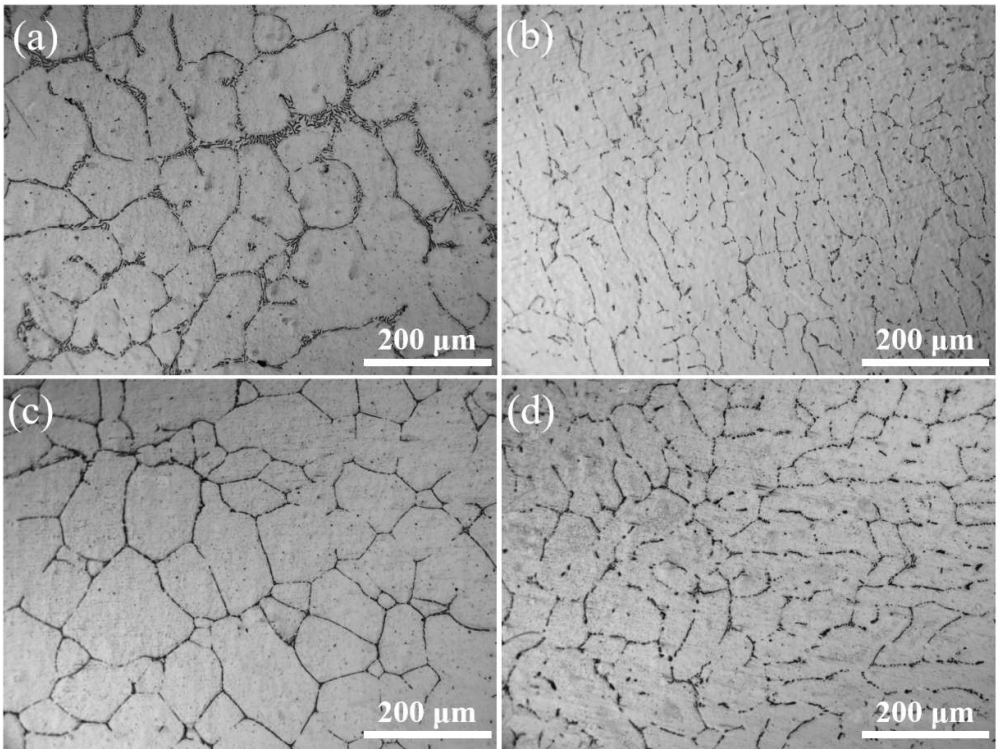

Fig. 1 Optical micrographs of the as-cast structure of (a) Al-0.4Fe; (b) Al-0.4Fe-0.1Zr; (c) Al-0.4Fe-0.2Er and (d) Al-0.4Fe-0.1Zr-0.2Er alloys.

Fig. 1 shows the microstructure of A1, A2, A3 and A4 alloys in as-cast condition. The base alloy (A1) contains typical dendrite structures with broadly eutectic region at grain boundaries (Fig. 1a), and the average grain size is about 132 µm. In the Zr-modified alloy (A2), significant grain refinement is, however, observed, with a grain size of ~81 µm in diameter and fine modified eutectic region at grain boundaries (Fig. 1b). The average grain size of Er-modified alloy (A3) and (Zr+Er)-modified alloy (A4) is approximately 140 µm and 102 µm, and the eutectic region is also modified, similar to that in A2. It means that the addition of 0.1 wt. % Zr results in grain refinement remarkably (decreases the average grain size by around 50 µm), however, Er addition does not exhibit the grain refinement. It can be also seen that the large eutectic region

existed at grain boundary in A1 (Fig. 1a) is modified by Zr and/or Er addition (Figs. 1b-d).

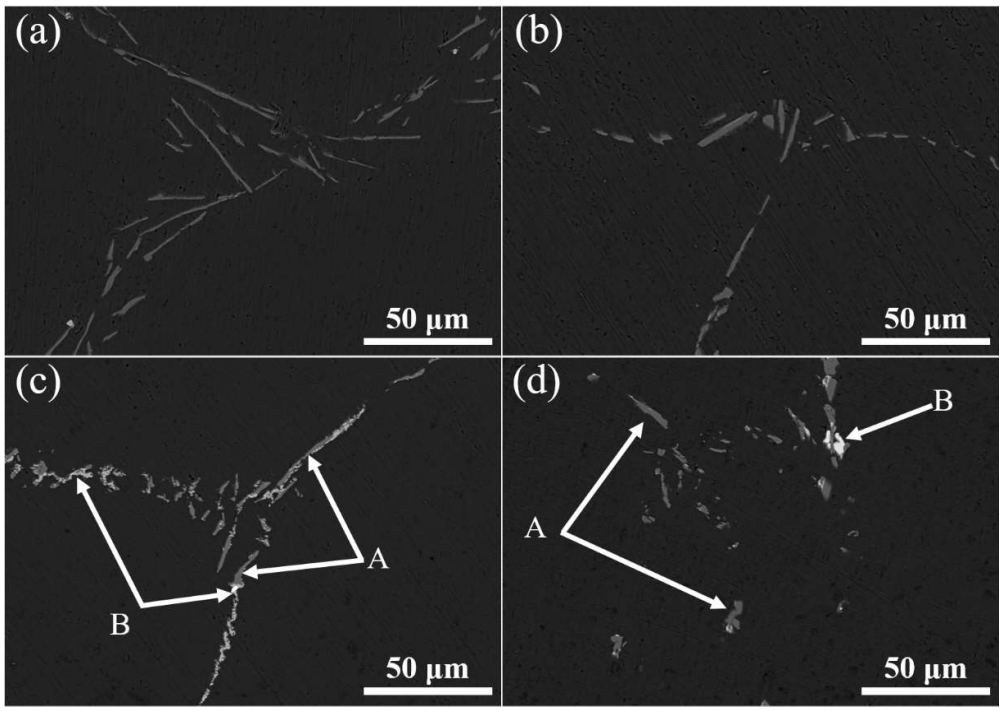

Fig. 2 SEM images of primary phases at grain boundary at four as-cast alloys, and the two types of particles with gray or bright contrast are pointed out by A or B plus arrows, respectively. Al-0.4Fe; (b) Al-0.4Fe-0.1Zr; (c) Al-0.4Fe-0.2Er and (d) Al-0.4Fe-0.1Zr-0.2Er.

Fig. 2 displays the more detailed microstructure of eutectic region in the four as-cast alloys. The primary phases are coarse and have needle-like morphology in the base alloy (A1) (Fig. 2a). The needle-like phases have been modified into short rods appearance with Zr and Er additions, as shown in Figs. 2b-d, which has also been observed in previous studies [13, 14]. It should be noted that, two types of primary phases may be discerned in A3 and A4 (Figs. 2c and d), including gray phase with a characteristic “short rods” morphology (named type A) and bright phase (type B), as

indicated by the arrows in Figs. 2c and d. Another feature is that the bright phase is always attached to the gray phase. The distribution of length and aspect ratio of the gray primary particles is shown in Fig. 3. The results reveal remarkably refining and spheroidization of this kind of phase upon Zr and Er additions. For instance, the length of gray particles is in a range of 2 to 40 μm in A1, however, that in the modified alloys (A2, A3 and A4) changed into 1 to 15 μm (Fig. 3a). The aspect ratio of the primary gray particles in A1 is dispersed as 1~60, while that of the modified alloys is concentrated in 1~10 (Fig. 3b). On average, the primary gray particle in A1 has a length of 14.3 μm, and the aspect ratio is 24.1. In the modified alloys, the average length of the gray particle is reduced to 5.1 μm, 6.2 μm, and 5.8 μm for A2, A3 and A4, respectively, and the aspect ratio is reduced to 4.8, 4.7 and 3.4.

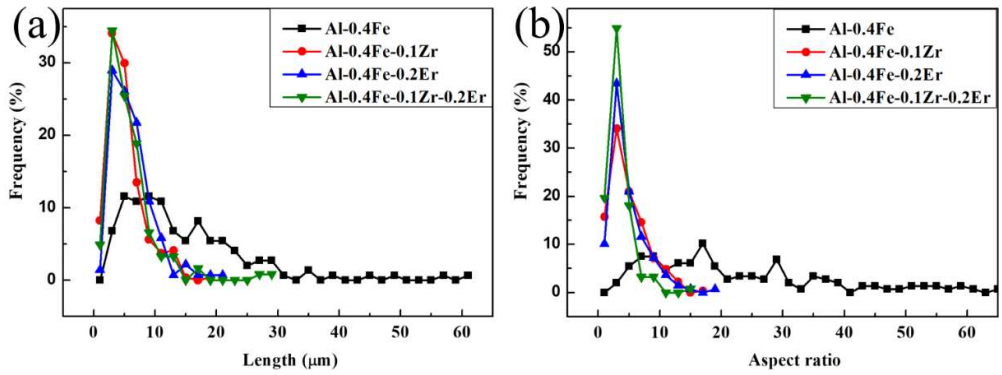

Fig. 3 Distribution of (a) length and (b) aspect ratio of primary gray particles in as-cast alloys.

Fig. 4 shows the SEM images of primary phases at the grain boundary and the corresponding EDS elemental mappings in the four as-cast alloys. The primary gray particles with needle-like morphology composed of Al and Fe elements are revealed (Fig. 4a), which is consistent with the results in Al-1Fe alloys [1, 3]. Zr addition could

modify such needle-like Al-Fe particles into short rods, but neither distribute in the Al-Fe particle nor form the Zr-rich primary particle, as supported in Fig. 4b. However, Er-rich particles are formed in the Er-added alloys (A3 and A4) as revealed by EDS mappings in Figs. 4c and d, corresponding to the bright particles in Figs. 2c and d. Compared with the color scale ranges of the two pictures in Figs. 4c and d, the color of Er-enriched dendrite region seems brighter and coverage scope appears larger in Fig. 4d, which indicates that Er-enriched primary phases at the interdendritic regions are relatively more in A4.

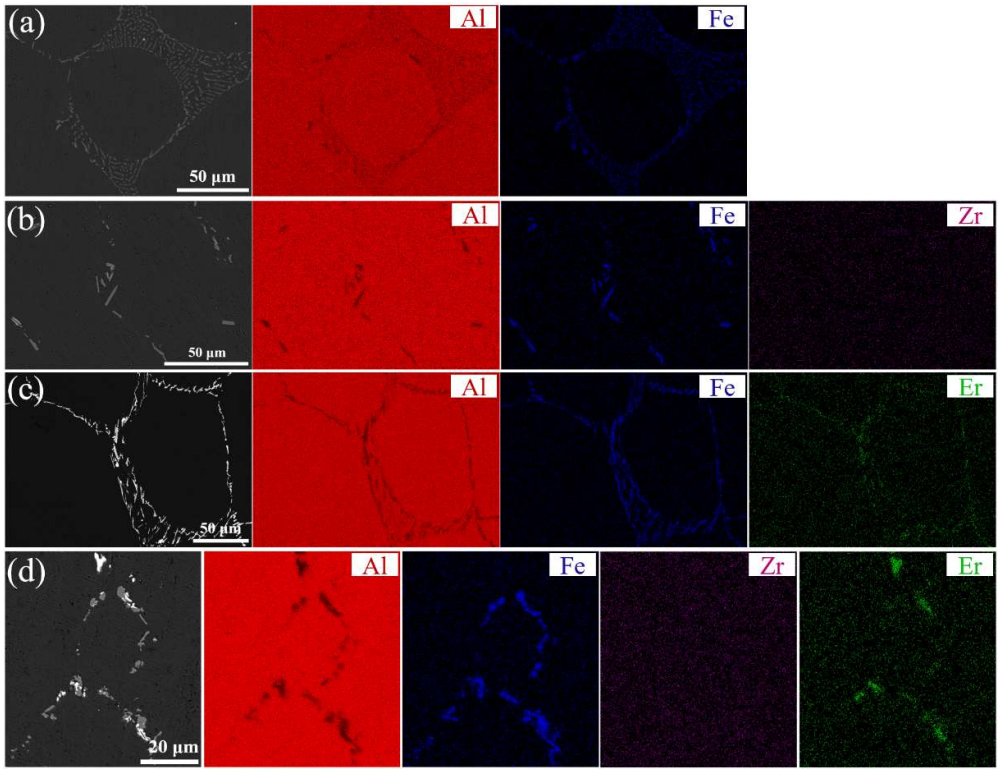

Fig. 4 SEM microstructure and corresponding EDS mappings of as-cast (a) Al-0.4Fe, (b) Al-0.4Fe-0.1Zr, (c) Al-0.4Fe-0.2Er and (d) Al-0.4Fe-0.1Zr-0.2Er alloys.

TEM observations were carried out to clarify the structure of two types of particles at grain boundary. An FIB technique was used to prepare a dedicated thin area including

the intended particles and the SEM image of a TEM foil is shown in Fig. 5a. Fig. 5b displays the STEM image taken in the same region as in Fig. 5a and the EDS results at points a, b, c and d are shown in Fig. 5c. It is revealed that the type A (gray, points a and d) mainly contains 75.3% Al and 24.7% Fe, and the type B (bright, point b) composes of 74.9% Al and 25.1% Er, respectively. Combined with the selected area electron diffraction (SAED) pattern in Figs. 5d-f, the type A, corresponding to the gray particles, is determined as Al_3Fe phase with monoclinic structure, while the type B, corresponding to bright particles, is Al_3Er phase. This Al_3Er particle is derived from the eutectic reaction $L \rightarrow \alpha\text{-}Al+Al_3Er$. The extra spots between the fundamental reflections in the <111> and <112> direction could be attributed to the long period superlattice of Al_3Er. Similarly, the long period superlattice of Al_3Ti and the extra reflections has been reported [15, 16].

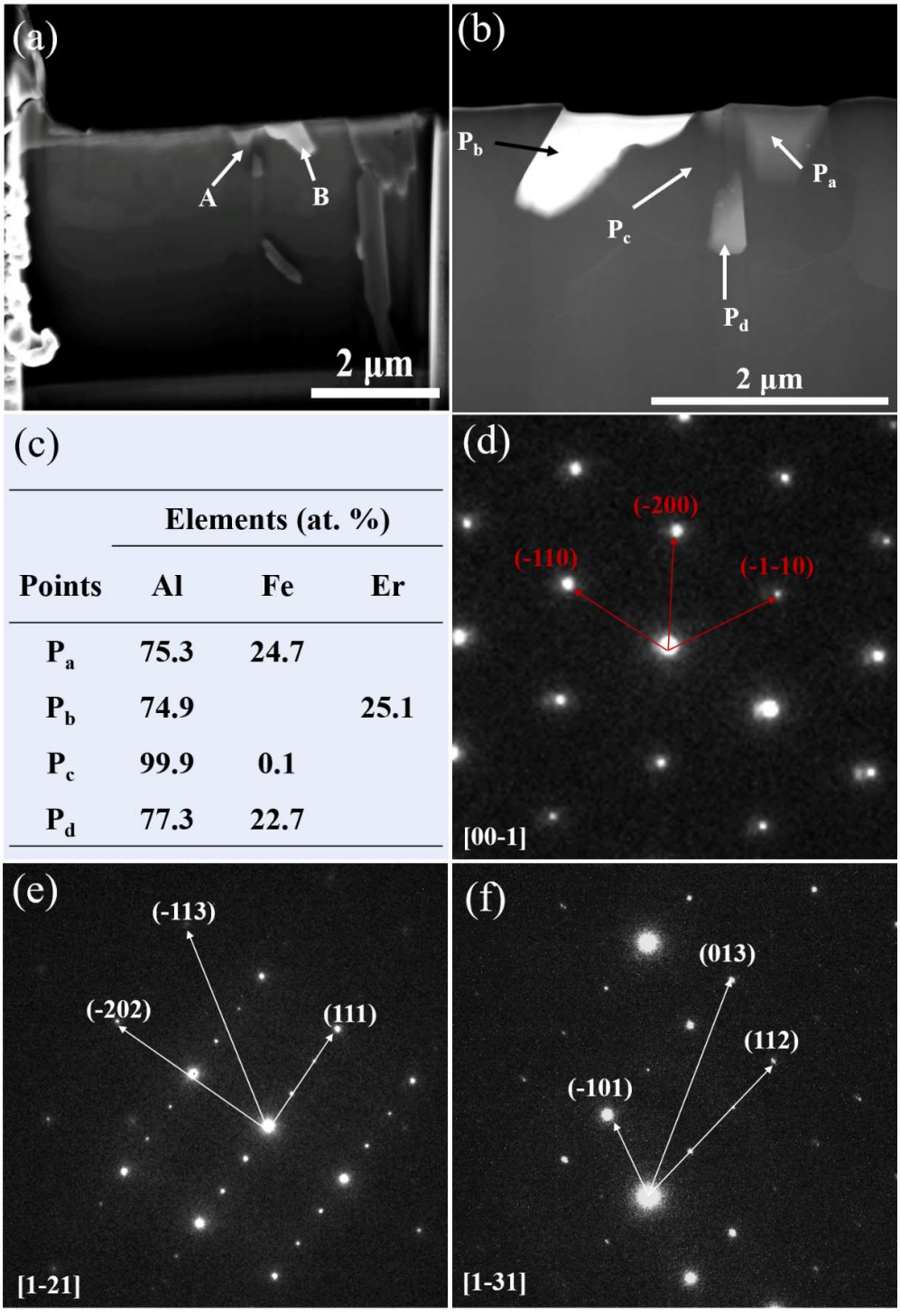

Points	Elements (at. %) Al	Fe	Er
P_a	75.3	24.7	
P_b	74.9		25.1
P_c	99.9	0.1	
P_d	77.3	22.7	

Fig. 5 (a) SEM image of a TEM foil obtained using FIB, (b) Typical STEM image of the two types of particles in the as-cast alloy, (c) EDS analysis at points a, b, c and d; (d) Corresponding SAED pattern of the Fe-rich particle at point a (Type A in Fig. 2); (e,

f) Corresponding SAED pattern of the Er-rich particle at point b (Type B in Fig. 2).

3.1.2 Microstructure after homogenization

The homogenization treatment at 600 ºC for 20 h has no obvious change on the primary Al_3Fe and Al_3Er phases, but facilitates the formation of spherical particles as shown in Figs. 6a and b. As can be seen in Fig. 6c, the EDS line scanning through the particle shows the enrichments of Er and Zr signals, and a peak for Er appears at the center of the profile and two intensive peaks for Zr on both sides, suggesting the core-shell structure of $Al_3(Zr,Er)$ particles. Similar spherical dispersoids particles with a core-shell structure were also observed in Al-Zr-Sc and Al-Zr-Er alloys [10, 11, 17].

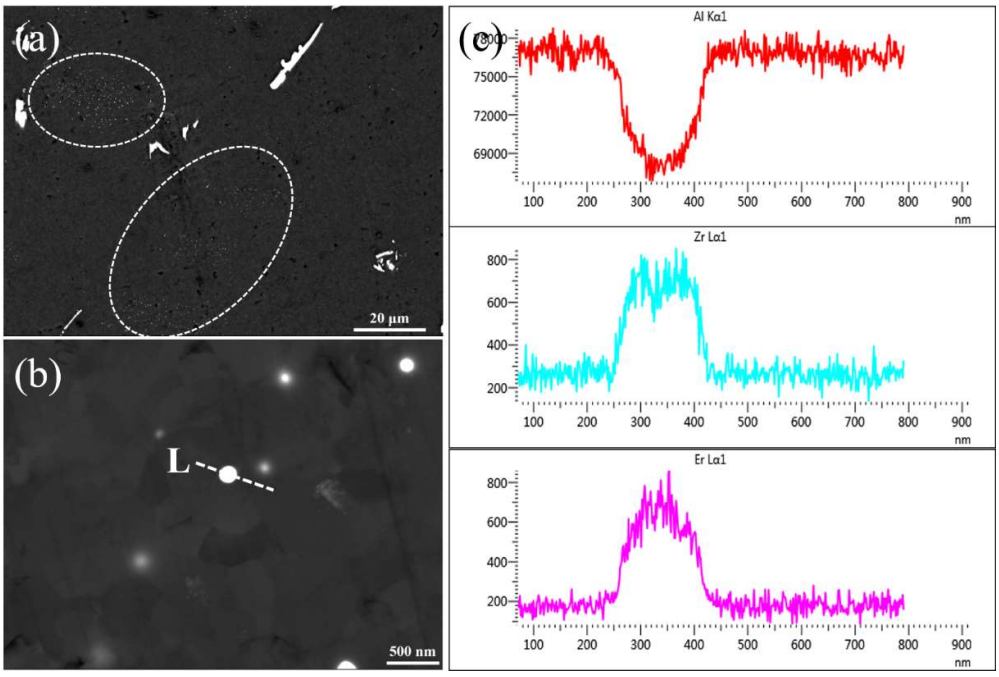

Fig. 6 SEM images and line scanning of particles in Al-0.4Fe-0.1Zr-0.2Er alloy after homogenization treatment at 600 °C for 20 h. (a) Homogenized microstructure of Al-0.4Fe-0.1Zr-0.2Er alloy, and the dispersoids particles are pointed out by white circles; (b) The dispersoids particles; (c) Composition profile along line L indicated in (b).

3.1.3 Microstructure after cold rolling and annealing

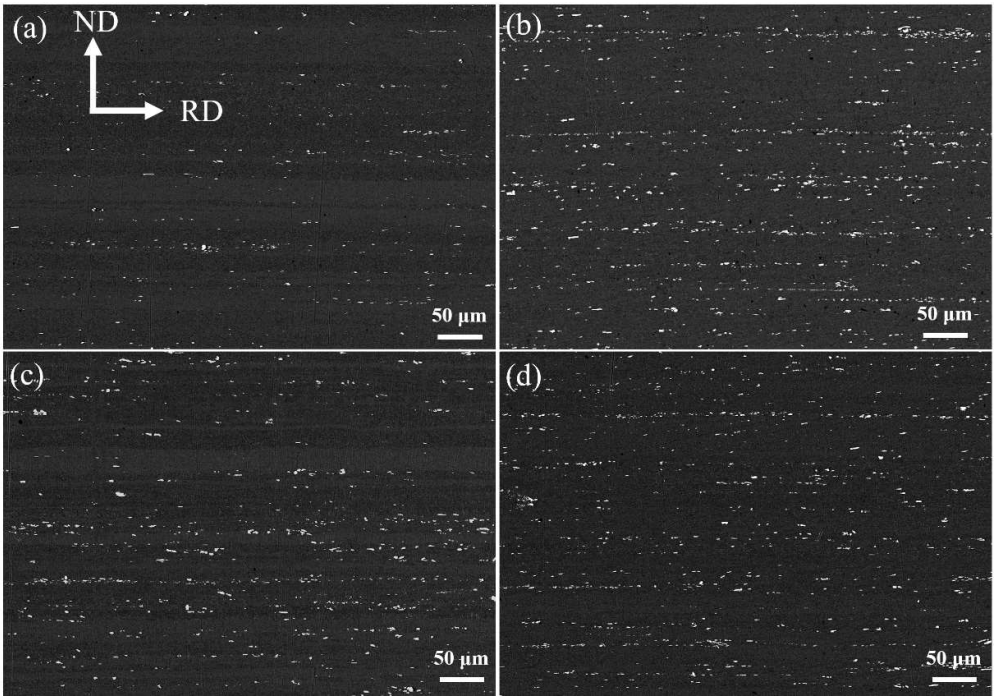

Fig. 7 SEM images of alloys after cold-rolling. (a) Al-0.4Fe, (b) Al-0.4Fe-0.1Zr, (c) Al-0.4Fe-0.2Er and (d) Al-0.4Fe-0.1Zr-0.2Er alloys.

The four alloys were carried out hot- and cold-rolling down to 2 mm in thickness, and the deformed microstructures are shown in Fig. 7. The α-Al grains are elongated with subgrains of width about 5 μm, and the primary particles are fractured into ~2μm in diameter and distributed at the grain boundaries along rolling direction.

The EBSD images from surface to center regions of samples annealed at 325 ℃ for 1 h are shown in Fig. 8. After annealing, A1 is obviously recrystallized, some of the subgrains boundaries disappear and some of the subgrains grow up into recrystallized grains with dimeter of 20~60 μm (Fig. 8a). A3 is also recrystallized, but with finer recrystallized grains with dimeter of 10~30 μm (Fig. 8c). However, A2 and A4 mainly have a fibrous unrecrystallized microstructure (Figs. 8b and d)). Based on the EBSD

analysis, recrystallization resistance of Al–0.4Fe alloy can be enhanced by Zr and Er. The effect of Zr is better than Er, and the synergetic effect of Zr and Er is better than the single addition.

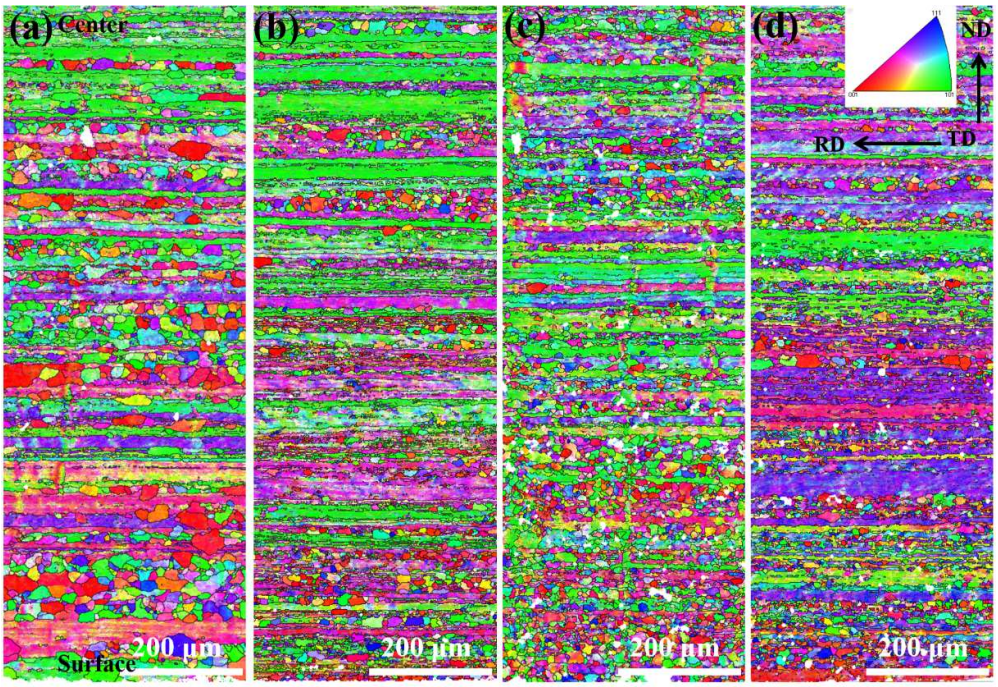

Fig. 8 EBSD images from surface to center regions of samples annealed at 325 °C for1 h. (a) Al-0.4Fe, (b) Al-0.4Fe-0.1Zr, (c) Al-0.4Fe-0.2Er and (d) Al-0.4Fe-0.1Zr-0.2Er alloys.

TEM images of the cold rolled alloys annealed at 325 °C for 1 h are shown in Fig. 9. Smooth and straight grain boundaries and few dislocations are observed in A1, shown in Fig. 9a. Low density of dislocation is observed within grain in A2 and A3 (Figs. 9b and c). High density dislocations and subgrains are visible within grains and near grain boundaries in A4 (Fig. 9d). Furthermore, dispersoids with diameter of 20~50 nm are found in A4 annealed at 325 °C for 1 h, shown in Fig. 10a. However, no dispersoids are observed in A1, A2 and A3 in this work, although similar experiments had been

performed. The dispersoids are referred as $Al_3(Zr,Er)$ based on the EDS mappings in Fig. 6 and Fig. 10, and they are located at or near gain boundaries.

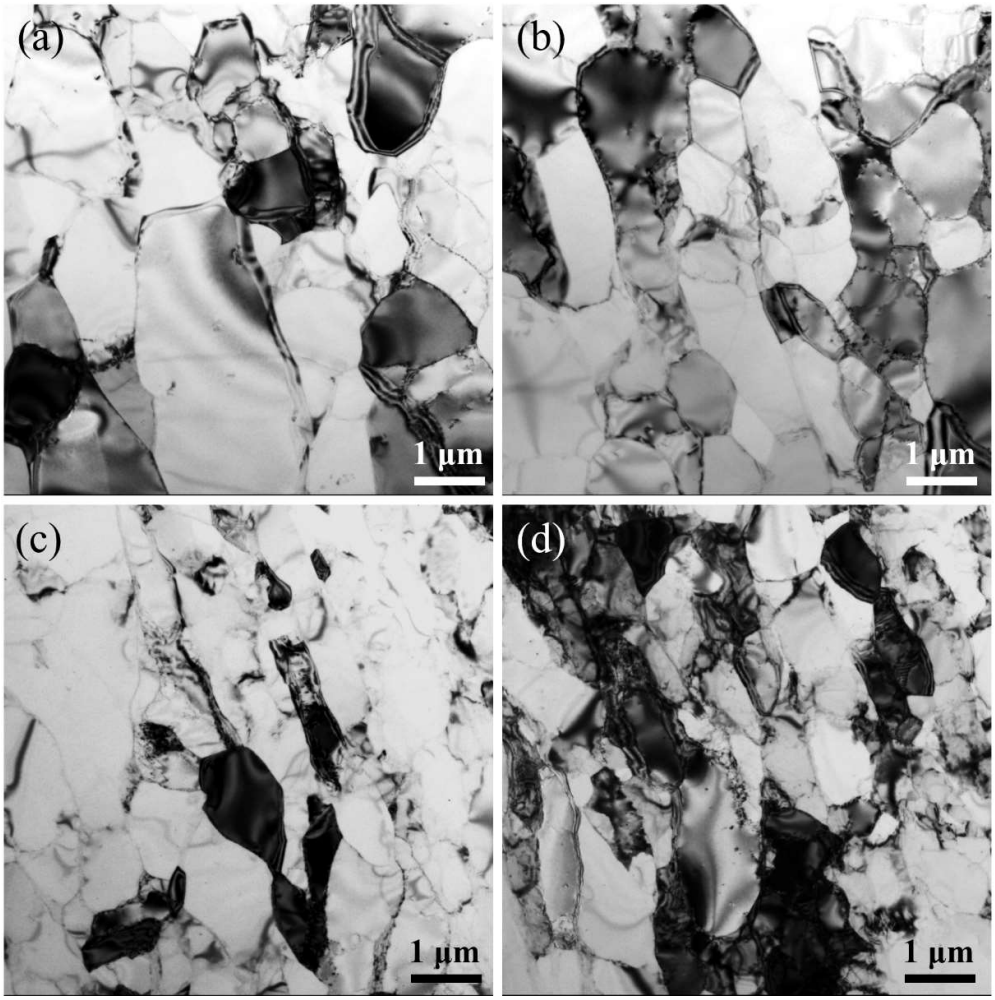

Fig. 9 TEM images of alloys annealed at 325 °C for1 h. (a) Al-0.4Fe, (b) Al-0.4Fe-0.1Zr, (c) Al-0.4Fe-0.2Er and (d) Al-0.4Fe-0.1Zr-0.2Er alloys.

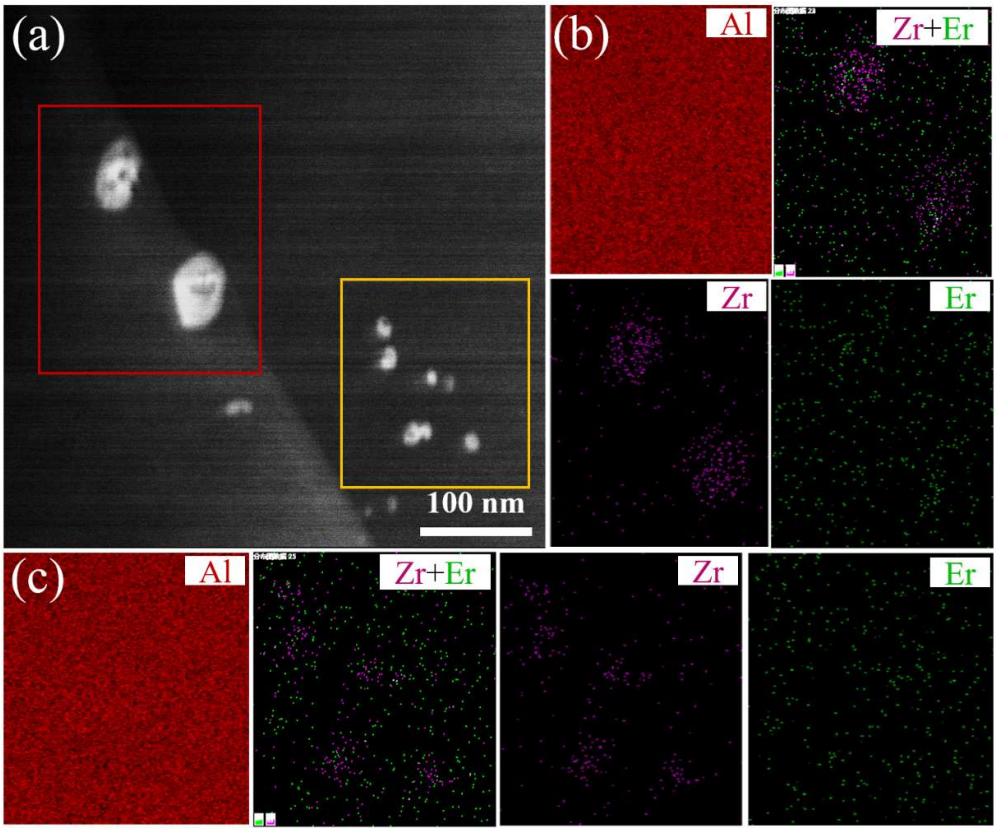

Fig. 10 STEM micrograph of Al-0.4Fe-0.1Zr-0.2Er alloy after annealed at 325 °C for 1 h (a) and EDS mappings of the marked regions by red box (b) and yellow box (c).

3.2 Mechanical properties and electrical conductivity

The microhardness and electrical conductivity of the four cold-rolled alloys annealed in the temperature range of 200 ºC to 400 ºC for 1 h were investigated and the softening curves are given in Fig. 11. In the cold-rolled state, the microhardness is over 43 HV. A3 and A4 have the higher microhardness, compared to A1 and A2, which is probably related to second phase strengthening (Fig. 11a). The microhardness of A1 moderately decreases when the annealing temperature increased from 200 °C to 275 °C, and an abrupt decrease occurs at an annealing temperature of 300 °C, then remains steady from 325 °C to 400 °C. The moderate decrease in microhardness may relate to

recovery, and the abrupt decrease at an annealing temperature of 300 °C may be attributed to the occurrence of recrystallization [18]. The microhardness of A2 after cold rolling is 44 HV, and remains stable at an annealing temperature of 200 ~300 °C, which is slightly higher than A1. During annealing at 200 ~400 °C, A4 shows the highest microhardness, which goes down at a slowest rate among the four studied alloys. Evidently, the addition of Zr and Er could delay the annealing softening effect and improve recrystallization temperature. Zr is more effective in restraining the softening than Er, and the synergetic effect of Zr and Er is better than the single addition. In addition, the additions of Zr and Er into Al-0.4Fe alloy can also affect evidently electrical conductivity, as shown in Fig. 11b. For example, the electrical conductivity of A2 and A4 with Zr is reduced to 58.7 % and 57.7 %IACS, respectively, as compared with 61.2 %IACS of A3 with single Er addition. It means that Zr could greatly reduce the electrical conductivity, but Er is just slightly. During annealing, the electrical conductivity increases. When the annealing temperature is increased to 300 °C, the electrical conductivity shows an abrupt increase. After annealing at 350 °C, the electrical conductivity tends to be stable with the further increase of temperature.

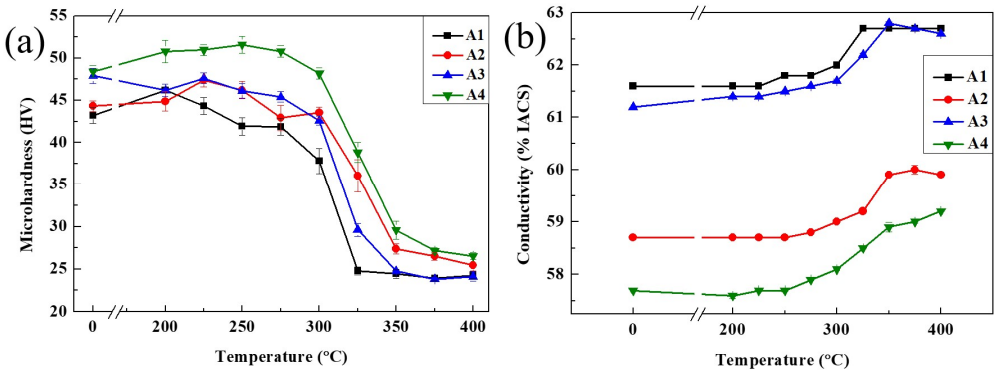

Fig. 11 The microhardness (a) and electrical conductivity (b) variations of cold-rolled

alloys annealed for 1 hour.

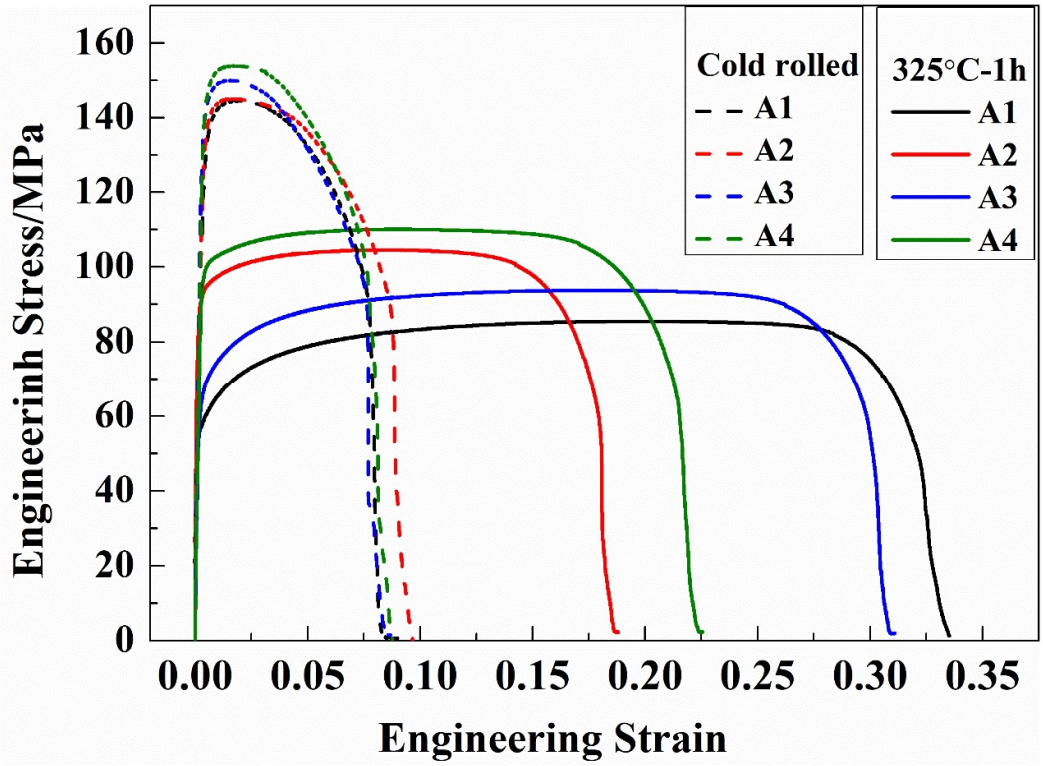

Fig. 12 Tensile properties of alloys in as cold-rolled state and after annealing at 325 °C for 1h.

Fig. 12 and Table 2 show the tensile properties of the alloys before and after annealing at 325 °C for 1 h. For the cold-rolled alloys, A1 and A2 exhibit similar strength of ~ 145 MPa, while a slight strength increase (~5-10 MPa) is occurred in A3 and A4 by Er addition. The ductility of A3 and A4 is somehow lower than that of A1 and A2. This is an indication that 0.2 wt. % Er single addition and the combined addition of 0.1 wt. % Zr and 0.2 wt. % Er in the base alloy could improve the strength, at an expense of a slight reduction in ductility. After annealing, the yield strength of four alloys has a serious drop which can be divided into two groups. A1 and A3 display 57% and 54% decrease, while A2 and A4 are 31% and 30%, respectively. This results

indicate that softening/recrystallization is more sensitive to Er instead of Zr addition. The reason is still unclear in this study. After annealing, the ductility of four alloys increased significantly, particularly, the elongation of A1 and A3 is more than three times that of cold-rolled alloys. Based on the above results, Zr and Er additions lead to an increase in microhardness, strength and a slight reduction in electrical conductivity. The best combination of strength and electrical conductivity is obtained in A3 after cold rolling. The yield strength, elongation and electrical conductivity of cold-rolled A3 is 145 MPa, 8% and 61.2 %IACS, while that of A1 is 136 MPa, 10% and 61.6 %IACS, respectively.

Table 2 Tensile properties of the as-rolled and heat treatment samples.

	Cold-rolled				After 325 °C for 1h			
Alloys	A1	A2	A3	A4	A1	A2	A3	A4
UTS [MPa]	145	145	150	154	86	105	94	110
$\delta_{0.2}$ [MPa]	136	137	145	146	59	95	67	102
EL [%]	10	10	8	8	34	19	31	23
Reduction in $\delta_{0.2}$ [%]					57	31	54	30

4. Discussion

4.1 Mechanism for refining and modifying

Table 3 shows the physicochemical parameters of related elements and their compounds [2, 14, 19-22]. Er has larger atomic weight and atomic radius and lower solubility in the α-Al crystals. Al_3Zr and Al_3Er have the same crystal structure (Fcc) and similar lattice constant compared to the α-Al (a = 0.4049 nm). Moreover, the element Zr exhibits terminal peritectic with Al at 660.8 °C, while the Al+Al_3Er, Al+Al_3Fe eutectics form at approximately 655 °C and 650 °C, respectively.

Zr atoms would be enriched in front of the α-Al grains during solidification due to

the large atomic weight and slow diffusion rate. Thus the undercooling increases, and the refinement effect is stronger [14]. Additionally, when the Zr content reaches composition of 0.11 wt. %, the fine Al_3Zr particles form from undercooled melt as the primary phase, then the Al_3Zr particles could act as the heterogeneous nuclei for the α-Al grains nucleating and increases nucleation rate and thus refines grain size remarkably at the process of subsequent solidification [23].

Referring to the Al-Er binary phase diagram, a eutectic reaction occurs at 655 °C at a composition of 6 wt. % Er, resulting in the formation of Al and the Al_3Er intermetallic phase. Analogously, the Er content must be higher than 6 wt. % for the formation of the Al_3Er as the primary phase and the nucleation sites. In the present work, the Er content is far below eutectic point. In consequence, Er refining to the grains in the alloy is negligible as revealed from Fig. 1. This phenomenon was also identified in the literatures [24, 25].

Table 3 Physicochemical parameters of related elements and their compounds.

Elements	Al	Fe	Zr	Er
Atomic radius (nm)	0.143	0.127	0.160	0.176
Atomic weight	26.98	55.85	91.22	167.26
Lattice constants of Al_3M (nm)	a = 0.405 b = 0.405 c = 0.405	a = 1.549 b = 0.808 c = 1.247	a = 0.407 b = 0.407 c = 0.407	a = 0.425 b = 0.425 c = 0.425
Reaction type		Eutectic	Peritectic	Eutectic
Reaction temp.(°C)		650.0	660.8	655.0
Composition at eutectic/peritectic point (wt. %)			0.28	6
Equilibrium maximum solid solubility (wt. %)		0.028	0.25	0

Furthermore, the additions of Zr and Er could modify the Al_3Fe phase (as shown in Figs. 2 and 4). On the one hand, Zr and Er atoms enriched at the front of the liquid/solid interface during solidification would prevent the growth of Al_3Fe phase

[13]. On the other hand, parts of the supersaturated Er atoms form Al_3Er phase, which is formed at α-Al/Al_3Fe interface to influence the growth of Al_3Fe phase. It's worth noting that Al_3Er is formed in the later stage of solidification at a relative lower eutectic temperature and higher eutectic composition. Therefore, the formed primary Al_3Er could only modify the morphology of Al_3Fe phase, but not for the grain size of Al matrix. In addition, the solubility of Er can be affected by other alloying elements in the multicomponent system [26, 27]. Zr was reported to reduce the solubility of Er in Al alloy [28]. More primary Al_3Er particles observed at the grain boundary in A4 comparing with A3 supports the conclusion in the literature [28].

4.2 Mechanical properties

The microstructure, such as grain size, shape and content of the secondary phase greatly influences the mechanical properties of the alloy. The contribution of possible mechanisms to the total hardening can be estimated as [29, 30]:

$$\sigma = \sigma_0 + \sigma_{gb} + \sigma_{ss} + \sigma_d + \sigma_p \quad (1)$$

Where σ is the total yield strength, σ_0 is the strength from Al matrix, σ_{gb} is the strengthening by interfaces and grain boundaries, σ_{ss} is the strength due to solute atoms dissolved in the matrix, σ_d is the strain strengthening, σ_p is the strength added by second phase.

In the cold-rolled samples, A3 and A4 display higher strength than A1 and A2. When adding 0.2 wt. % Er, Al_3Fe and Al_3Er phases are in the forms of needles, rods and blocks. After hot-and cold-rolling, the Al_3Fe and Al_3Er particles break up and change into finer particles, which distribute in Al matrix and lead to significantly

strengthening (σ_p). The contribution of refined α-Al grains (σ_{gb}) and fractured Al_3Fe and Al_3Er phases (σ_p) also make the strength of A4 improved. Furthermore, the nanosized $Al_3(Zr,Er)$ particles are obstacles to the movement of dislocation and most dislocations do not free themselves from powerful pining, thus the strength of cold-rolled A4 is also improved owing to the $Al_3(Zr,Er)$ dispersoids. In general, the deference of strength in cold rolled samples is dominantly from second phases (σ_p). As shown in Table 4, the contribution from Al_3Fe exists in all the four alloys, while the contribution of Al_3Er is in A3 and A4, and $Al_3(Zr,Er)$ is just in A4, where Al_3Fe and Al_3Er refer to broken primary phases, and $Al_3(Zr,Er)$ is nanosized dispersoids, respectively.

Table 4 The contributions of secondary particles to the strength of cold rolled samples. Note: "+" means contribution, and "--" means no contribution.

	Contributions		
Alloys	Al_3Fe	Al_3Er	$Al_3(Zr,Er)$
A1	+	--	--
A2	+	--	--
A3	+	+	--
A4	+	+	+

The decreased strength after annealing would be due to recovery and recrystallization. During annealing, recovery and recrystallization occur, resulting in absorption of dislocation and decreased strength. The good strength of A2 and A4 after annealing at 325 °C for 1h is due to strain strengthening from the rest deformed structure, as shown in Figs. 8d and d. In addition, the strength of A4 keeps higher after annealing at 325 °C for 1h, which relates to the high density of dislocations and subgrains, as shown in Fig. 9d. The lower strength of A1 and A3 results from a high

proportion of recrystallized structure (Figs. 8a and c). The recovery and recrystallization process is related to the movement of dislocations and grain boundaries. The excellent recrystallization resistance of A4 is caused by the strong pinning effects of Al_3(Zr,Er) precipitates on dislocations or subgrain boundaries during recovery and recrystallization [31]. The phenomenon that Al_3M (M=Zr/Sc/Er/Hf) inhibited recrystallization of aluminum alloy was also reported in Al-Zr-Sc and Al-Zr-Mn alloys [17, 32, 33].

4.3 Electrical conductivity

The electrical conductivity decreases with the addition of Zr and Er, particularly for Zr added alloys. For instance, the electrical conductivity of A2 and A4 is much lower than A3 (Fig. 11b). The obvious different effect of Zr and Er should be associated with their different solid solubility in Al matrix. Knipling et al. [34, 35] have reported that the maximum solubility of Zr and Er in the Al matrix was 0.25 wt. % and 0, respectively. Thus, in the case of adding 0.1 wt. % Zr, almost all the Zr atoms are dissolved in Al matrix which increases electrical scattering. Hence the electrical conductivity of A2, A4 is only 58.7 %IACS and 57.7 %IACS, lower by 4.7% and 6.3% compared to A1 (61.6 %IACS), respectively. The weak influence from Er is due to the very low fraction of Er atoms in Al matrix.

The lower electrical conductivity in the cold-rolled alloys can be associated with the gradually increasing lattice distortion during cold rolling, in which a few atoms shift away from the original balance positions. Therefore, electron scattering should be intensified due to the increasing density of defects, leading to a decreased electrical

conductivity. During the annealing process, the electrical conductivity increases with the increasing annealing temperature (Fig. 11b). On the one hand, annealing leads to a decrease in dislocation density, which reduces scattering effect of the electron wave, decreases electrical resistivity and improves electrical conductivity. On the other hand, Zr and Er atoms in the Al matrix are precipitated, reducing the lattice distortion, which weakens scattering effect of the electron wave, leading to an increase of the electrical conductivity.

5. Conclusions

(1) The grain size of Al-0.4Fe alloy is obviously refined by Zr addition. Zr and Er elements modify the morphology of Al_3Fe phases. The needle-like Al_3Fe phases are modified to fine and short rods particles. Zr promotes the formation of primary Al_3Er phase and $Al_3(Zr,Er)$ precipitates in Al-0.4Fe-0.15Zr-0.25Er alloy during solidification and homogenization, respectively.

(2) Zr and Er additions could increase microhardness and strength with a slight reduction in electrical conductivity. The best combination of strength and conductivity in Al-0.4Fe-0.2Er alloy after cold rolling is obtained: the yield strength of 145 MPa, the elongation of 8% and the electrical conductivity of 61.2 %IACS.

(3) Zr and Er could improve recrystallization resistant capability of Al-0.4Fe alloy. The effect of Zr is better than Er, and the synergetic effect of Zr and Er is better than the single addition.

Acknowledgements

This work was supported by the Fundamental Research Funds for the Central

Universities of China (Grant No. 2018CDGFCL0002 and 2019CDQYWL029), the National Natural Science Foundation of China (Grant No. 51871035 and No. U1710124) and the Foundation for Innovative Research Groups of the National Natural Science Foundation of China (Grant No. 51421001).

References

[1] Jy. Zhang, Xy. Jiang, My. Ma, B. Jiang, B. Wang, Dq. Yi, Effect of scandium micro-alloying on the creep resistance properties of Al-0.7Fe alloy cables, Materials Science & Engineering A. 699 (2017) 194-200.

doi: 10.1016/j.msea.2017.05.088.

[2] X. Wang, R.G. Guan, R.D.K. Misra, Y. Wang, H.C. Li, Y.Q. Shang, The mechanistic contribution of nanosized Al3Fe phase on the mechanical properties of Al-Fe alloy, Materials Science and Engineering: A. 724 (2018) 452-460.

doi: 10.1016/j.msea.2018.04.002.

[3] Z.M. Shi, K. Gao, Y.T. Shi, Y. Wang, Microstructure and mechanical properties of rare-earth-modified Al−1Fe binary alloys, Materials Science and Engineering: A. 632 (2015) 62-71.

doi: 10.1016/j.msea.2015.02.068.

[4] S.X. Luo, Z.M. Shi, N.Y. Li, Y.M. Lin, Y.H. Liang, Y.D. Zeng, Crystallization inhibition and microstructure refinement of Al-5Fe alloys by addition of rare earth elements, Journal of Alloys and compounds. 789 (2019) 90-99.

doi: 10.1016/j.jallcom.2019.03.071.

[5] S. Mondol, S. Kashyap, S. Kumar, K. Chattopadhyay, Improvement of high temperature strength of 2219 alloy by Sc and Zr addition through a novel three-stage heat treatment route, Materials Science and Engineering: A. 732 (2018) 157-166.
doi: 10.1016/j.msea.2018.07.003.

[6] L. Fu, Y. Li, F. Jiang, J. Huang, G. Xu, Z. Yin, On the role of Sc or Er micro-alloying in the microstructure evolution of Al-Mg alloy sheets during annealing, Materials Characterization. 157 (2019) 109918.
doi: 10.1016/j.matchar.2019.109918.

[7] A.G. Mochugovskiy, A.V. Mikhaylovskaya, N.Y. Tabachkova, V.K. Portnoy, The mechanism of $L1_2$ phase precipitation, microstructure and tensile properties of Al-Mg-Er-Zr alloy, Materials Science and Engineering: A. 744 (2019) 195-205.
doi: 10.1016/j.msea.2018.11.135.

[8] E.Gariboldi, M. Colombo, A. Morri, Influences of different Zr additions on the microstructure, room and high temperature mechanical properties of an Al-7Si-0.4Mg alloy modified with 0.25%Er, Materials Science & Engineering A. 713 (2018) 151-160.
doi: 10.1016/j.msea.2017.12.068.

[9] D.C. Dunand. R.A. Karnesky, D.N. Seidman, Evolution of nanoscale precipitates in Al microalloyed with Sc and Er, Acta Materialia. (14) 57 (2009) 4022-4031.
doi: 10.1016/j.actamat.2009.04.034.

[10] K.Y. Gao, S.P. Wen, Y. Li, H. Huang, Z.R. Nie, Synergetic effect of Er and Zr on the precipitation hardening of Al–Er–Zr alloy, Scripta Materialia. (7) 65 (2011) 592-

595.

doi: 10.1016/j.scriptamat.2011.06.033.

[11] K.Y.Gao, S.P. Wen, H. Huang, W. Wang, Z.R. .Nie, Precipitation evolution in Al–Er–Zr alloys during aging at elevated temperature, Journal of Alloys and compounds. 574 (2013) 92-97.

doi: 10.1016/j.jallcom.2013.03.237.

[12] H.C. Fang, H. Chao, K.H. Chen, Effect of Zr, Er and Cr additions on microstructures and properties of Al–Zn–Mg–Cu alloys, 610 (2014) 10-16.

doi: 10.1016/j.msea.2014.05.021.

[13] Z.M. Shi, Y.H. Liang, G.W. Li, R.Y. Zhang, G. Zhao, Effects of Er addition on the crystallization characteristic and microstructure of Al-2wt. %Fe cast alloy, Journal of Alloys and compounds. 781 (2019) 235-244.

doi: 10.1016/j.jallcom.2018.12.063.

[14] Z.M. Shi, Q. Wang, G. Zhao, R.Y. Zhang, Effects of erbium modification on the microstructure and mechanical properties of A356 aluminum alloys, Materials Science & Engineering A. 626 (2015) 102-107.

doi: 10.1016/j.msea.2014.12.062.

[15] A. Pasturel, C. Colinet, Ab initio calculation of the formation energies of $L1_2$, $D0_{22}$, $D0_{23}$ and one dimensional long period structures in $TiAl_3$ compound, Intermetallics. 10 (2002) 751-764.

doi:

[16] D.B. Williams, Transmission electron microscopy :a textbook for materials science,

(1996) 264.

doi:

[17] R-g. Guan, H-m. Jin, W. Jiang, X. Wang, X. Wang, , Y-x. Wang, Z. Li, J. Zhang, H. Liu, Quantitative contributions of solution atoms, precipitates and deformation to microstructures and properties of Al–Sc–Zr alloys, Transactions of Nonferrous Metals Society of China. (5) 29 (2019) 907-918.

doi: 10.1016/s1003-6326(19)65000-4.

[18] W. Wang, S.P. Wen, W.H. Zhao, X.L. Wu, K.Y. Gao, H. Huang, Z.R. Nie, Precipitation hardening and recrystallization behavior of Al-Mg-Er-Zr alloys, 687 (2016) 143-151.

doi: 10.1016/j.jallcom.2016.06.045.

[19] M.J. Kaufman, J.D. Cotton, Microstructural Evolution in Rapidly Solidified AI-Fe Alloys: An Alternative Explanation, Metallurgical Transactions A. 22 (1991) 927-934.

doi:

[20] D.C. Dunaud, K. E. Knipling, D.N. Seidman, Criteria for developing castable, creep-resistant aluminum-based alloys – A review, 97 (2006) 246-265.

doi:

[21] F.H. Fang, O.N. Senkov, V.V. Stolyarov, R.Z. Valiev, J. Liu, Microstruture of aluminum-iron alloys subjected to severe plastic deformation, Scripta Materialia. 37 (1998) 1511-1516.

doi: 10.1016/S1359-6462(98)00073-6.

[22] Dx. Yang, Xy. Li, Dy. He, H. Huang, Effect of minor Er and Zr on microstructure and mechanical properties of Al–Mg–Mn alloy (5083) welded joints, Materials Science and Engineering: A. 561 (2013) 226-231.
doi: 10.1016/j.msea.2012.11.002.

[23] X. Huang, Q. Pan, B. Li, Z. Liu, Z. Huang, Z. Yin, Effect of minor Sc on microstructure and mechanical properties of Al–Zn–Mg–Zr alloy metal–inert gas welds, Journal of Alloys and compounds. 629 (2015) 197-207.
doi: 10.1016/j.jallcom.2014.11.227.

[24] Y. Deng, G. Zhang, Z. Yang, Gf. Xu, Microstructure characteristics and mechanical properties of new aerospace Al-Mg-Mn alloys with Al3(Sc1−xZrx) or Al3(Er1−xZrx) nanoparticles, Materials Characterization. 153 (2019) 79-91.
doi: 10.1016/j.matchar.2019.04.032.

[25] Z.B. Xing, S.P. Wen, H. Huang, B.L. Li, W. Wang, Z.R. Nie, The effect of erbium on the microstructure and mechanical properties of Al–Mg–Mn–Zr alloy, Materials Science and Engineering: A. (1-2) 516 (2009) 42-49.
doi: 10.1016/j.msea.2009.02.045.

[26] Y. Zhang, K. Gao, S. Wen, H. Huang, W. Wang, Z. Zhu, Z. Nie, D. Zhou, Determination of Er and Yb solvuses and trialuminide nucleation in Al–Er and Al–Yb alloys, Journal of Alloys and compounds. 590 (2014) 526-534.
doi: 10.1016/j.jallcom.2013.11.211.

[27] Z.G. Wu, M. Song, Y.H. He, Effects of Er on the microstructure and mechanical properties of an as-extruded Al–Mg alloy, Materials Science and Engineering: A. (1-2)

504 (2009) 183-187.

doi: 10.1016/j.msea.2008.11.030.

[28] W. Kang, H.Y. Li, S.X. Zhao, Y. Han, C.L. Yang, G. Ma, Effects of homogenization treatments on the microstructure evolution, microhardness and electrical conductivity of dilute Al-Sc-Zr-Er alloys, Journal of Alloys and compounds. 704 (2017) 683-692.

doi: 10.1016/j.jallcom.2017.02.043.

[29] I.F. Mohamed, Y. Yonenaga, S. Lee, K. Edalati, Z. Horita, Age hardening and thermal stability of Al–Cu alloy processed by high-pressure torsion, Materials Science and Engineering: A. 627 (2015) 111-118.

doi: 10.1016/j.msea.2014.12.117.

[30] M. Zha, Xt. Meng, HM. Zhang, XH. Zhang, HL. Jia, YJ. Li, JY. Zhang, HY. Wang, QC. Jiang, High strength and ductile high solid solution Al–Mg alloy processed by a novel hard-plate rolling route, Journal of Alloys and compounds. 728 (2017) 872-877.

doi: 10.1016/j.jallcom.2017.09.017.

[31] W.W. Zhou, B. Cai, J. Li, Z.X. Liu, S. Yang, Heat-resistant Al–0.2Sc–0.04Zr electrical conductor, Materials Science and Engineering: A. 552 (2012) 353-358.

doi: 10.1016/j.msea.2012.05.051.

[32] Zh. Jia, Gq. Hu, B. Forbord, J.K. Solberg, Effect of homogenization and alloying elements on recrystallization resistance of Al–Zr–Mn alloys, Materials Science and Engineering: A. (1-2) 444 (2007) 284-290.

doi: 10.1016/j.msea.2006.08.097.

[33] Zh. Jia, J. Royset, J.K. Solberg, Q. Liu, Formation of precipitates and

recrystallization resistance in AlScZr alloys, Nonferrous Met. Soc. China. 22 (2012) 1866-1871.

doi: 10.1016/S1003-6326(11)61399-X.

[34] Jy. Zhang, Hx. Wang, Dq. Yi, B. Wang, Hsh. Wang, Comparative study of Sc and Er addition on microstructure, mechanical

properties, and electrical conductivity of Al-0.2Zr-based alloy cables, Materials Characterization. 145 (2018) 126-134.

doi: 10.1016/j.matchar.2018.08.037.

[35] Rg. Guan, Yf. Shen, Zhy. Zhao, X. Wang, A high-strength, ductile Al-0.35Sc-0.2Zr alloy with good electrical conductivity strengthened by coherent nanosized-precipitates, Journal of Materials Science & Technology. (3) 33 (2017) 215-223.

doi: 10.1016/j.jmst.2017.01.017.